Supplement of Atmos. Chem. Phys., 21, 12479–12493, 2021
https://doi.org/10.5194/acp-21-12479-2021-supplement

Atmospheric Chemistry and Physics
Open Access
EGU

Supplement of

Variability in black carbon mass concentration in surface snow at Svalbard

Michele Bertò et al.

Correspondence to: Andrea Spolaor (andrea.spolaor@cnr.it) and Michele Bertò (michele.berto@gmail.it)

1. Calibration of the SP2

The empirical calibration of the SP2, performed using size selected fullerene soot particles is linear up to 500 nm, and the assumption is that it is also linear beyond that size (and the corresponding mass). However, when a massive particle enters the laser beam the incandescence signal might saturate the detector; therefore, in this analysis only the particles below 700 nm were considered. The evaluation of the BC mass for the samples showing a BC geometric mean mass equivalent diameter above 300/400 nm might therefore be more influenced resulting in underestimation of the mass. However, the evaluation of the missing mass is beyond the scope of this manuscript and require further analyses. The losses of mass due to the presence of undetected small particles, below 80/70 nm of MED, is not significant given that the geometric mean of the MED of the mass size distributions is always above 150 nm.

2. Possible interferences during the SP2 rBC mass concentration in Arctic snow

The surface snow of the Svalbard archipelago is normally characterized by high content of sea salt particles, for example those containing Na, due to its geographical position surrounded by the ocean. The Na concentration in the samples analyzed in this work is, on average, about 500 ng g^{-1}. We cannot exclude that the rBC mass concentration variability for the 85-days experiment presented in this work might have been slightly influenced by the Na content (tracer of sea salt deposition), however no clear relation appeared from the comparison between the rBC and the Na mass concentrations during the "85 days" experiment (Fig. SI 3). As a precaution, all the samples from the 3-days experiments were diluted five times with Milli-Q water prior to the SP2 analyses. The SP2 instrumental performances during the analyses, in terms of laser power and incandescence signal quality, were monitored and constant. At the best of our knowledge, no study focusing on the possible effects of the Na particles on the rBC mass concentration retrieved from the SP2 has been published in the literature. Further analyses of snow samples collected in areas characterized by a high influence of marine-like aerosols could shed light on the effects of salt particles on the rBC mass and number concentration via SP2 measurements, as well as establishing a shared procedure to avoid measuring artifacts.

Mineral dust particles might have an influence on the SP2 measurements, depending on their chemical and physical properties. Currently, the literature lacks investigation on these specific SP2-mineral dust particles interactions. However, a few studies on snow and ice samples measured with an SP2 take the assumptions that mineral dust particles are not detected by the SP2 as incandescence signals, but only as scattering signals (Kaspari et al., 2011). Recent studies, based on atmospheric measurements suggest that the SP2 rBC mass concentration measurement can potentially be interfered by the presence of metals and metals-oxide (Moteki et al., 2017), of volcanic ashes or of dust (Kupiszewski et al., 2016).

3. Ancillary measurements for the 3-days samples: Na, Mn, EC, OC

Ancillary data were measured/gathered for the 3-days experiment in order to strengthening the interpretations even though they were not considered in the statistical exercise. The Mn concentrations are considered to be a good proxy for mineral dust aerosols (Baker et al., 2006). The Mn concentration profile was compared with that of the coarse mode particles concentration showing a very similar behavior and suggesting a common source.A similar pattern is also clearly visible for all the various chemical species.

Every six hours a surface snow sample was collected in parallel to that of the hourly sampling. The melt snow volume of these samples were of about 1618 ± 290 mL cm^3 and they were used for TC (Total Carbon), EC (Elemental Carbon) and OC (Organic Carbon) measurements. Results are shown in Fig. SI 4. A different profile is shown for the three compounds compared to that of the rBC mass concentration. As reported above, the two measuring techniques are different and, in particular, the size range of particles detected by the two instruments is different, from 80 to 600 nm for the SP2 whereas a much broader dimensional spectrum for the Sunset, potentially explaining part of the observed difference. Interestingly, the EC daily values increased of one order of magnitude, from 1 to 10 μg l^{-1}, during the sampling period, showing a maximum during the precipitation episode. For more info and results about the comparison between rBC and EC snow/ice measurement see Sigl et al. (2018). On the contrary, the OC atmospheric concentration showed a decreasing trend with the highest values at the beginning of the sampling period and the lowest at the end, similarly to the atmospheric eBC behavior. Remarkably, the highest OC concentration was found in the same sample were the highest concentration of all the other measured compounds was found (at the very beginning of the snow episode) suggesting a common atmospheric scavenging process, although not above the average for the rBC mass concentration.

4. Sodium/manganese concentrations measurements

Concentrations of sodium (Na) and manganese (Mn) were also determined as tracer of sea spray emission and dust deposition by Inductively Coupled Plasma Sector Field Mass Spectrometry (ICP-SFMS; Element2, ThermoFischer, Bremen, Germany) equipped with a cyclonic Peltier-cooled spray chamber (ESI, Omaha, USA). The sample flow was maintained at 0.4 mL min^{-1}. Detection limits, calculated as three times the standard deviation of the blank, were 0.5 ng g^{-1} for ^{23}Na and 0.3 ng g^{-1} for Mn. The residual standard deviation (RSD) for Na and Mn ranged between 2–5%.

5. Back trajectories calculation and Potential Source Contribution Function analysis

Air mass back-trajectories (BT) were calculated using the NOAA ARL HYSPLIT 4 rev. 513 transport model (Stein et al., 2015). Global Data Assimilation System (GDAS) meteorological input fields with 0.5x0.5 degree resolution and a propagation time of 240 hours was employed. The trajectories were calculated every hour for an endpoint of 500 m above ground level in Ny-Ålesund. A

potential source contribution function (PSCF) analysis has been applied to the BTs exploiting a specifically developed FORTRAN computer code (Petroselli et al., 2018). That analysis considered BC concentration measured in the air by both AE31 and PSAP. Briefly, the method calculates the probability of finding a source of a particular pollutant on a certain region by superimposing grid cells to it and estimating the fraction of the total time spent on each cell by trajectories associated with a high concentration measured at the receptor site. The 90th percentile was used to define the high concentration limit and cells of 3 x 3 degrees (lat-long) were exploited in the calculation of probabilities. Details of the PSCF methodology employed here are described in Petroselli et al., (2018). The data of the active fires, covering the last 12 days before the sampling day, are from the MODIS active fire products (https://firms. modaps.eosdis.nasa.gov/firemap/), offered by NASA LANCE.

In order to evaluate the impact of the Eurasian fires on the measured atmospheric eBC concentrations, a thorough back-trajectories analysis was performed for both the snow-sampling periods. Results of PSCF analysis on eBC (Figures SI 1a, SI 1b and SI 1c; open-fire episodes are reported in red on the map) show a clear maximum of probability over the Central Siberia, which appears to be the major source area of eBC in this period over Ny-Ålesund. Some false positive source areas are located in Greenland, the Queen Elisabeth Islands region and the Arctic Ocean, even if associated to a lower probability. These artifacts are due to the persistent circulation of BTs in the Arctic vortex. An example of BTs generating the above salient features in the PSCF plot is reported in Figure SI 1b. Here BTs are shown to loop for few days around the Arctic at high altitudes and afterwards to descend at lower altitudes over Siberia, just four days before reaching Ny-Ålesund on April 22, when a clear maximum in the eBC trend has been recorded. Back trajectory analysis supports the idea that the peaks of eBC in the atmosphere in early spring are directly correlated with long-range transport from Eurasia, whereas the peaks in late May and June are much lower in intensity and they seem to be more related to a Western circulation pattern.

The results of BT analysis for the 3-days experiment are reported in Figure SI 2, suggesting that the air masses were persistently circulating in the polar vortex causing a similar weather condition within the three days of the experiment.

Table S1. Abakus Klotz selected dimensional bins.

Channel	Size (µm)	11	2.2	22	6.4
1	0.8	12	2.4	23	7.1
2	0.9	13	2.6	24	7.8
3	1	14	2.9	25	8.6
4	1.1	15	3.2	26	9.5
5	1.2	16	3.5	27	10.5
6	1.3	17	3.9	28	11.6
7	1.4	18	4.3	29	12.8
8	1.6	19	4.8	30	14.1
9	1.8	20	5.3	31	15.5
10	2	21	5.8	32	80

Figure S1. a) Potential source contribution function analysis (PSCF) of eBC recorded in the 85-days experiment (8 April-29 June). 10 days back-trajectories for two selected days: b) 22 April and c) 23 May. Four BTs were calculated for the two selected days, with a 6 hours interval. The red crosses represent the fires taking place during the last 10 days (data from the MODIS active fire products (https://firms. modaps.eosdis.nasa.gov/firemap).

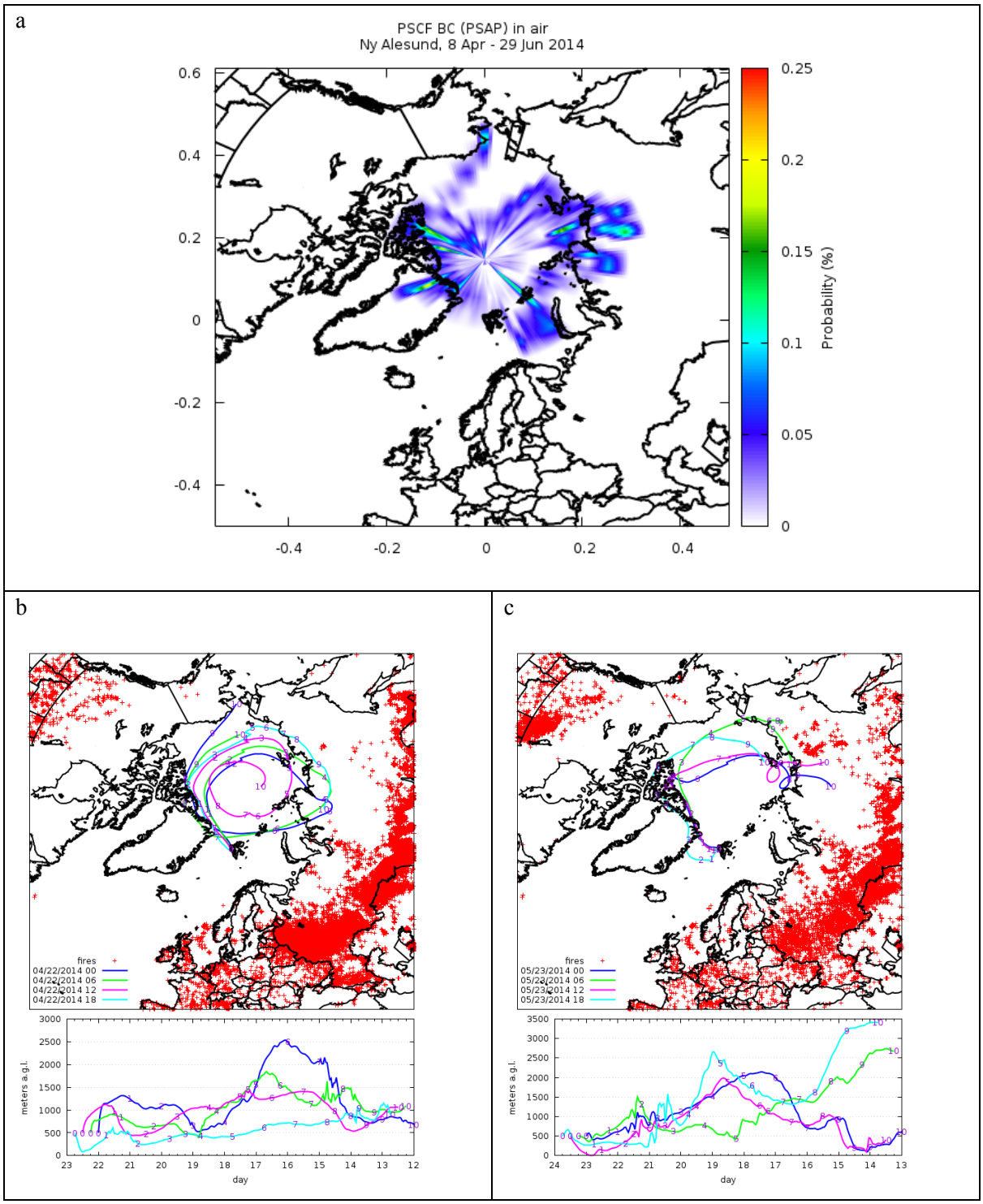

Figure S2. 10 days back-trajectory results for the 3-days experiment. The red crosses represent the fires taking place during the last 10 days (data from the MODIS active fire products (https://firms.modaps.eosdis.nasa.gov/firemap/).

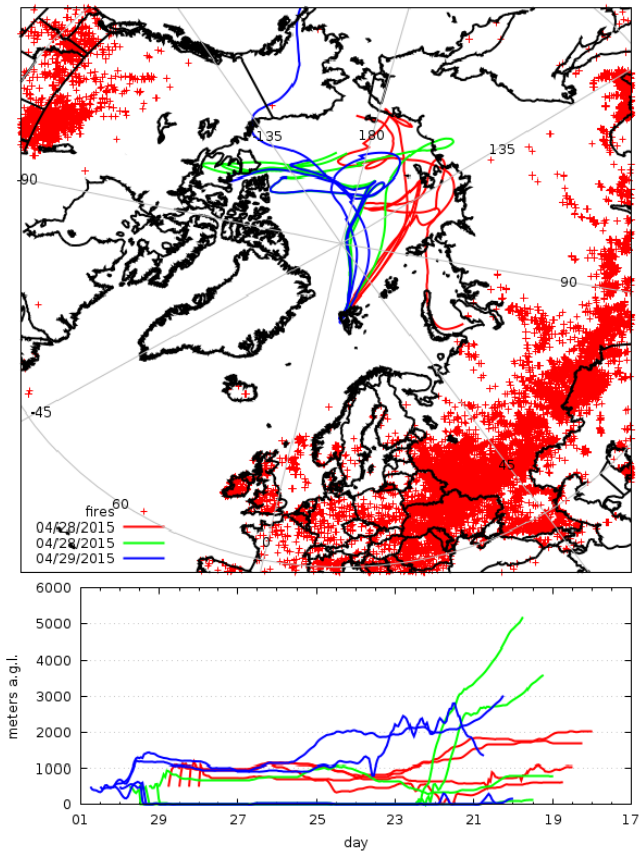

Figure S3. Results for the 85-days experiment from ancillary measurements. Upper panel: rBC mass concentration (gray line), Na concentration (red line) and conductivity (green line). Lower panel: atmospheric eBC mass concentration (black line) and ammonia as measured at the Zeppelin station, Svalbard (gray bars).

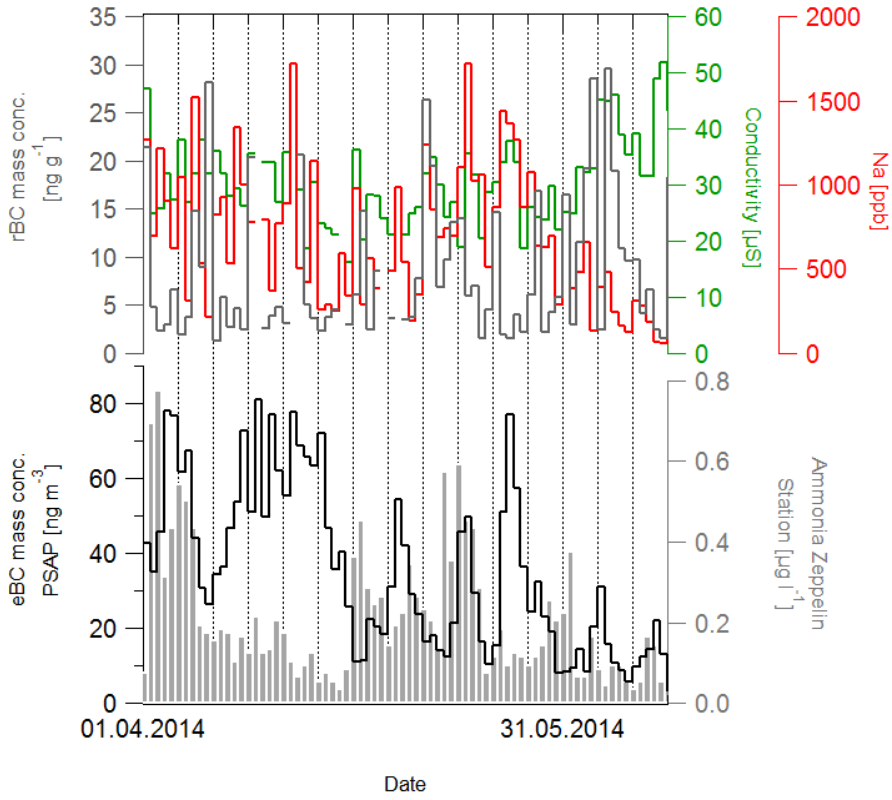

Figure S4. Ancillary measurements for the 3-days experiments. Uppermost panel: manganese (Mn, dark-yellow line) mass concentration and the coarse mode particles number (blu line). Second uppermost panel: rBC mass concentration (gray line) with sodium (Na) concentration (red line) and conductivity (green line). Second lowermost panel: atmospheric eBC mass concentration (black line), snow OC concentration (blue bars) and daily average of atmospheric ammonia as measured at the Zeppelin station (gray bars). Lowermost panel: TC (red bars), OC (blue bars) and EC (green bars) and EC daily average (black line).

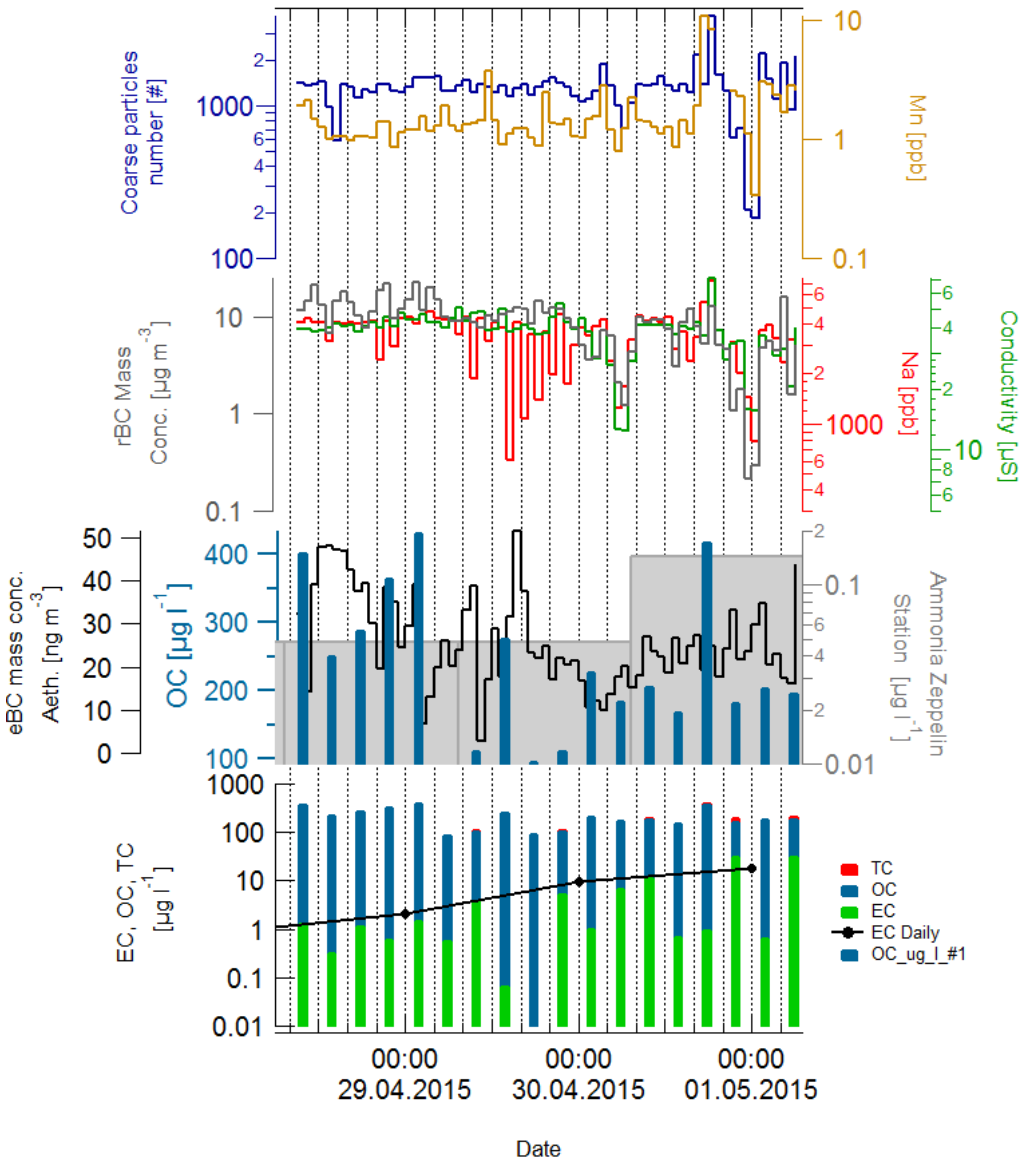

References:

Kaspari, S. D., Schwikowski, M., Gysel, M., Flanner, M. G., Kang, S., Hou, S. and Mayewski, P. A.: Recent increase in black carbon concentrations from a Mt. Everest ice core spanning 1860–2000 AD, Geophysical Research Letters, 38(4), doi:10.1029/2010GL046096, 2011.

Kupiszewski, P., Zanatta, M., Mertes, S., Vochezer, P., Lloyd, G., Schneider, J., Schenk, L., Schnaiter, M., Baltensperger, U., Weingartner, E. and Gysel, M.: Ice residual properties in mixed-phase clouds at the high-alpine Jungfraujoch site, Journal of Geophysical Research: Atmospheres, 121(20), 12,343-12,362, doi:10.1002/2016JD024894, 2016.

Moteki, N., Adachi, K., Ohata, S., Yoshida, A., Harigaya, T., Koike, M. and Kondo, Y.: Anthropogenic iron oxide aerosols enhance atmospheric heating, Nature Communications, 8, 15329, doi:10.1038/ncomms15329, 2017.

Sigl, M., Abram, N. J., Gabrieli, J., Jenk, T. M., Osmont, D. and Schwikowski, M.: 19th century glacier retreat in the Alps preceded the emergence of industrial black carbon deposition on high-alpine glaciers, The Cryosphere, 12(10), 3311–3331, doi:https://doi.org/10.5194/tc-12-3311-2018, 2018.

Petroselli, C., Crocchianti, S., Moroni, B., Castellini, S., Selvaggi, R., Nava, S., Calzolai, G., Lucarelli, F. and Cappelletti, D.: Disentangling the major source areas for an intense aerosol advection in the Central Mediterranean on the basis of Potential Source Contribution Function modeling of chemical and size distribution measurements, Atmospheric Res., 204, 67–77, doi:10.1016/j.atmosres.2018.01.011, 2018.

Stein, A. F., Draxler, R. R., Rolph, G. D., Stunder, B. J. B., Cohen, M. D. and Ngan, F.: NOAA's HYSPLIT Atmospheric Transport and Dispersion Modeling System, Bull. Am. Meteorol. Soc., 96(12), 2059–2077, doi:10.1175/BAMS-D-14-00110.1, 2015.